explaining 60 or 56% of the variance. Natural enemies in fragmented habitats are more likely to be lost than their phytophagous prey because population growth starts only after the successful establishment of prey populations, and populations will be smaller in small habitat islands. The result is that food chains should be shorter in small islands than in larger habitats (*18*).

Small populations isolated by disturbed environments are characteristic features of the agricultural landscape. The time between population crashes (determined by cutting of vegetation or ploughing) may often be shorter than the recovery time of natural enemies, especially when they prey on only one or two species (*19*). In such situations of local loss and recolonization, predator-prey systems and multitrophic cascade effects begin to depend on metapopulation processes (*20*), such that only mobile and abundant natural enemies can regulate actual or potential pests.

In addition, release of dominant competitors from natural control may cause competitive exclusion of herbivores. Competition is a structuring factor in endophagous but not ectophagous insect communities (*21*), and as expected, we found competition to be important for the insects spatially restricted to the clover flowerheads. Extinction of weak competitors resulting from the release of dominant ones may be a further indirect consequence of reduced biocontrol.

We conclude that habitat fragmentation affects natural enemies more than their phytophagous hosts. Fragmentation reduced not only biodiversity but also the rate of predation or parasitism. The rate of parasitism is linked to the success of biocontrol; habitat isolation can be expected to release herbivores from the control of predators or parasitoids. Accordingly, designs of the agricultural landscape that maintain habitat connectivity may contribute to the biocontrol of potential or actual pests.

REFERENCES AND NOTES

1. J. M. Diamond and R. M. May, in *Theoretical Ecology*, R. M. May, Ed. (Blackwell, Oxford, 1981), pp. 228–252; D. S. Wilcowe, C. H. McLellan, A. P. Dobson, in *Conservation Biology: The Science of Scarcity and Diversity*, M. E. Soulé, Ed. (Sinauer, Sunderland, MA, 1986), pp. 237–256.
2. D. R. Strong, J. H. Lawton, T. R. E. Southwood, Eds., *Insects on Plants* (Blackwell, Oxford, 1984); R. M. May, *Science* **241**, 1441 (1988).
3. J. LaSalle and J. D. Gauld, *Redia* **74**, 315 (1991).
4. H. Zwölfer, *Schriftenr. R. Naturschutz Landschaftspflege München* **12**, 81 (1980).
5. The mean proportion of short-winged individuals for the five controls was 55.6% (SD = 8.1%) and for the 13 clover islands, 2.9% (SD = 4.8%). Data were from 241 well-developed specimens reared after dissection of the stems (76 for the controls and 165 for the clover islands).
6. W. Stein, *Z. Angew. Entomol.* **66**, 372 (1970).
7. Demographic and genetic contributions from conspecific immigrants reduced extinction rates of insular populations as predicted by a modification of the MacArthur-Wilson model of island biogeography and supported by the distribution of arthropod species among isolated thistles [J. H. Brown and A. Kodric-Brown, *Ecology* **58**, 445 (1977)].
8. A. Sih, P. Crowley, M. McPeek, J. Petranka, K. Strohmeier, *Annu. Rev. Ecol. Syst.* **16**, 269 (1985).
9. H.-J. Greiler, S. Vidal, T. Tscharntke, in *Proceedings of the 4th European Congress of Entomology and of the 13th Internationales Symposium für die Entomofaunistik Mitteleuropas*, Gödöllö, Hungary, 1 to 6 September 1991, L. Zambori and L. Peregovitz, Eds. (Hungarian National History Museum, Budapest, 1992), p. 299.
10. B. Hawkins and P. Gross, *Am. Nat.* **139**, 417 (1992).
11. J. LaSalle, in *Hymenoptera and Biodiversity*, J. LaSalle and J. D. Gauld, Eds. (CAB International, Wallingford, United Kingdom, 1993), pp. 197–215.
12. B. A. Hawkins, M. B. Thomas, M. E. Hochberg, *Science* **262**, 1429 (1993).
13. N. E. Stork, *Biol. J. Linn. Soc.* **35**, 321 (1988).
14. J. H. Myers, C. Higgins, E. Kovacs, *Environ. Entomol.* **18**, 541 (1989).
15. Samples of 200 vetch pods were taken from each of the 16 old meadows differing in size (300 to 800,000 m^2, $n = 16$) in June 1993. The number of herbivore species ($Y = 1.82 + 0.17\ln X$, $F = 21.7$, $r^2 = 0.607$, $P < 0.001$, $n = 16$), number of parasitoid species ($Y = -0.27 + 0.25\ln X$, $F = 9.2$, $r^2 = 0.397$, $P < 0.01$, $n = 16$), and percent parasitism of the seed-feeding weevil *A. ochropus* ($Y = 10 + 5.3\ln X$, $F = 11$, $r^2 = 0.440$, $P < 0.01$, $n = 16$) were closely correlated with habitat size.
16. S. L. Pimm, *The Balance of Nature* (Univ. of Chicago Press, Chicago, 1991).
17. J. H. Lawton, in *Species Richness, Population Abundance, and Body Sizes in Insect Communities: Tropical Versus Temperate Comparisons*, P. W. Price, T. Lewingsohn, W. Fernandes, W. Benson, Eds. (Wiley, New York, 1991), pp. 71–90; K. J. Gaston and J. H. Lawton, *Nature* **331**, 709 (1988).
18. T. W. Schoener, *Ecology* **70**, 1559 (1989).
19. Frequent disturbances of phytotelmata (water-filled plant bodies) result in predator removal and two–trophic level systems [S. L. Pimm and R. L. Kitching, *Oikos* **50**, 302 (1987)]. Similarly, increasing patchiness in goldenrod fields leads to more frequent local explosions of aphid populations [P. Kareiva, *Nature* **326**, 388 (1987)].
20. A. D. Taylor, *Biol. J. Linn. Soc.* **42**, 305 (1991); T. Tscharntke, *Ecology* **73**, 1689 (1992); *Conserv. Biol.* **6**, 530 (1992).
21. R. Karban, *Ecology* **70**, 1028 (1989).
22. Comments of B. A. Hawkins, W. J. Boecklen, and R. Brandl greatly improved this report. S. Vidal identified the Chalcidoidea and M. Čapek the Braconidae. Supported by the German Science Foundation (Deutsche Forschungsgemeinschaft, DFG).

24 January 1994; accepted 28 April 1994

Structure of the Equine Infectious Anemia Virus Tat Protein

D. Willbold, R. Rosin-Arbesfeld, H. Sticht, R. Frank, P. Rösch*

Trans-activator (Tat) proteins regulate the transcription of lentiviral DNA in the host cell genome. These RNA binding proteins participate in the life cycle of all known lentiviruses, such as the human immunodeficiency viruses (HIV) or the equine infectious anemia virus (EIAV). The consensus RNA binding motifs [the trans-activation responsive element (TAR)] of HIV-1 as well as EIAV Tat proteins are well characterized. The structure of the 75–amino acid EIAV Tat protein in solution was determined by two- and three-dimensional nuclear magnetic resonance methods and molecular dynamics calculations. The protein structure exhibits a well-defined hydrophobic core of 15 amino acids that serves as a scaffold for two flexible domains corresponding to the NH_2- and COOH-terminal regions. The core region is a strictly conserved sequence region among the known Tat proteins. The structural data can be used to explain several of the observed features of Tat proteins.

Equine infectious anemia virus Tat protein is a monomeric protein of 75 amino acids (*1*). From sequence comparisons of lentiviral Tat proteins, it was concluded that immunodeficiency virus Tat protein sequences are in general subdivided into several regions: an NH_2-terminal region, a Cys-rich region, a core region, a basic region, a Glu-rich region, and a COOH-terminal region (*2*). The Cys-rich region is thought to bind two Zn^{2+} ions (*3*), and the basic region is involved in binding of the TAR RNA recognition sequence (*4*). The Cys-rich region and a sequence homologous to the HIV-1 Tat COOH-terminus are not present in the EIAV Tat protein. The highly conserved core region encompasses amino acids Tyr^{35} through Tyr^{49} in EIAV Tat protein. In this study we used both chemically synthesized (*5*) and bacterially expressed protein (*6*).

The nuclear Overhauser enhancement spectroscopy (NOESY) cross-peak pattern (Fig. 1) shows that the protein has a tendency to form weak helices from amino acid Ala^{10} to Asn^{13} as well as through the core and basic regions (that is, amino acids His^{36}

D. Willbold, H. Sticht, P. Rösch, Lehrstuhl für Biopolymere und Bayreuther Institut für Makromolekülforschung, Universität Bayreuth, D-95440 Bayreuth, Germany.
R. Rosin-Arbesfeld, Sackler Faculty of Medicine, Department of Human Microbiology, Tel Aviv University, Ramat-Aviv, 69978 Tel Aviv, Israel.
R. Frank, Zentrum für Molekularbiologie Heidelberg, D-69120 Heidelberg, Germany.
*To whom correspondence should be addressed.

to Arg^{61}, the latter helical part interrupted by the region from Leu^{45} to Asp^{48}). The intensity of cross peaks suggesting helical secondary structures (that is, NH-C_{α}H, i, $i + 3$ and C_{α}H-C_{β}H, i, $i + 3$) is very low. Therefore, it may be deduced that at any given time a small subset of the total number of protein molecules displays at least local helix-type conformation. These helix-type structures thus form possible limit structures of the protein (*7*).

Three-dimensional (3D) structures were calculated from the experimental distance constraints with the X-PLOR 3.1 molecular dynamics program (*8*). Initially, structures with an approximately correct 3D fold were calculated from structures with random backbone conformations with the standard simulated annealing (SA) and refinement protocols, with minor modifications. These structures were then refined again with the same SA protocol and a refinement protocol with the use of explicit electrostatic interaction terms. The calculation protocol and summary statistics for the structure calculations are given in Table 1.

The 3D structure of the EIAV Tat protein is subdivided into domains of different flexibility. Amino acids Tyr^{35} through Tyr^{49}, which form a hydrophobic core domain, provide a scaffold for the flexible NH_2-terminal, basic, and Glu-rich parts of the amino acid sequence. This core region comprises only 20% of the whole sequence, and the number of intraresidual and sequential nuclear Overhauser effects (NOEs) in the core region is also about 20% of the total number of NOEs in these categories. In contrast, 35% of the medium-range and 63% of the long-range NOEs were observed entirely within the core region. All long-range NOEs and 46% of the medium-range NOEs originate from amino acids in the core region. This hydrophobic core domain is also well defined by the nuclear magnetic resonance (NMR) data according to the molecular dynamics calculations, with a root-mean-square deviation (RMSD) of about 0.04 nm for the core-region backbone atoms (Fig. 2), compared to the corresponding RMSD of more than 0.47 nm for the whole protein backbone (Table 1). The flexibility of the structure is also evidenced by the lack of slowly exchanging protons. The architecture of this core is made possible only because the strictly conserved residue Gly^{46} allows a structural turn at this position (Fig. 3).

The sequence regions essentially correspond to structural domains (Fig. 4): The basic region wraps around the core domain, and the NH_2-terminal as well as the COOH-terminal region form large loop domains that fold back to the hydrophobic core, placing the NH_2- and COOH-termini at close distance. The latter, more flexible regions are anchored to the hydrophobic core by way of the following amino acids (observed NOESY cross peaks

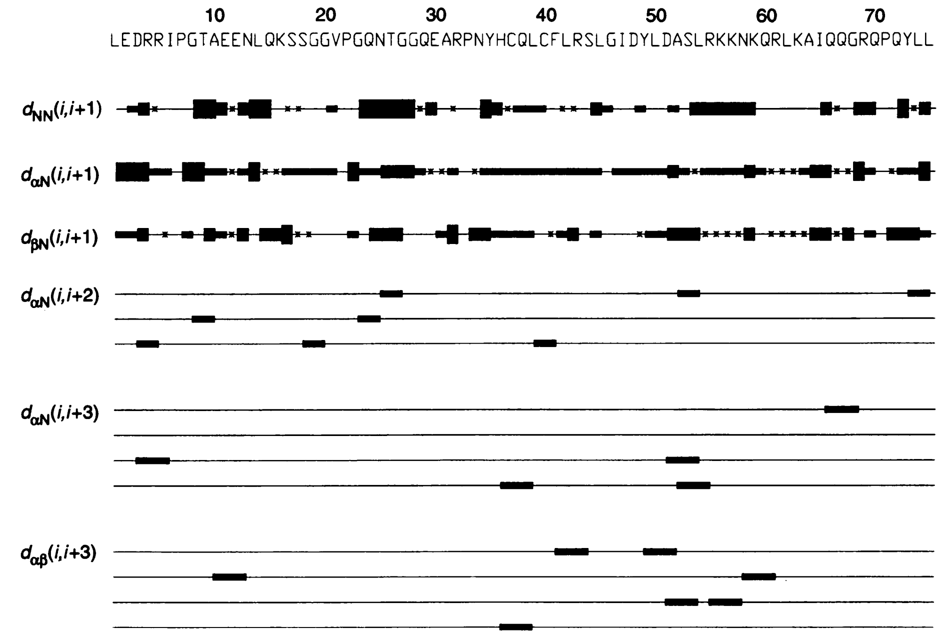

Fig. 1. NOESY connectivities involving backbone protons for amino acids i and j with $|i-j| < 4$. The height of the bars symbolizes the relative strength (weak, medium, strong) of the cross peaks in a qualitative way. Amino acids are labeled according to the one-letter convention (*16*) (Fig. 5). The following 600-MHz NMR spectra were used for the sequence-specific assignment of spin systems and the evaluation of NOESY distance constraints: Double quantum filtered–COSY, TOCSY with mixing times of 80, 100, 150, and 200 ms, respectively, NOESY with mixing times of 150 and 300 ms, respectively, and 3D HMQC with ^{15}N-labeled protein. Data for long-range NOEs ($|i-j| > 5$) were extracted from both NOESY spectra, whereas data for sequential, short-range, and medium-range NOEs were extracted from the 150-ms NOESY spectrum only. The sample contained an approximately 8 mM concentration of bacterially expressed protein in 15 mM potassium phosphate buffer (pH 6.3), H_2O-^2H_2O (90 and 10%, respectively) solution.

Table 1. X-PLOR parameters after simulated annealing refinement. Sequential assignments of amino acid spin systems were made from two-dimensional correlated spectroscopy (COSY), NOESY, and total coherence spectroscopy (TOCSY) with the published standard procedures (*19, 20*)

RMSD from ideality	
NOEs (nm)	0.0140
Angles (degrees)	1.445
Bonds (nm)	0.0014
Improper (degrees)	1.310
Average energies (kJ/mol)	
E_{NOE}	3497.4
E_{VDW}	−688.3
E_{Total}	−338.5
RMSD among backbone structures (nm)	
Whole protein	0.471
Hydrophobic core, Tyr^{35} to Tyr^{49}	0.042

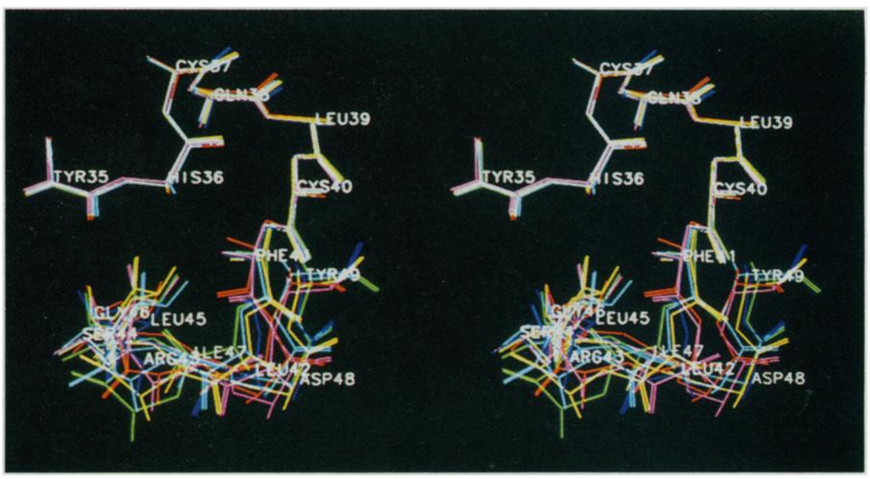

Fig. 2. Structure of the hydrophobic core of the protein, Tyr^{35} to Tyr^{49}. Shown is the superposition of the protein backbone of six structures selected out of a total of 11 by the criteria described in Table 1.

in parentheses): Asp[3] ($C_\beta H$ to NH of Tyr[49]); Gln[70] ($C_\gamma H$ to $C_\epsilon H$ of Tyr[49]); Pro[71] ($C_\beta H$ to $C_\epsilon H$ of Tyr[49]); Tyr[73] ($C_\delta H$ to $C_\delta H$ of Tyr[49]); Leu[74] ($C_\alpha H$ to NH of Ile[47]).

Sequence alignments such as in Fig. 5 or in (*2*) suggest that the general structural features of the EIAV Tat protein are also valid for the more intensely studied HIV-1 Tat protein, and several biochemical data on Tat proteins can be explained on the basis of the present structure of EIAV Tat. Mutations in the core region influence the trypsin digestion pattern of HIV-1 Tat protein (*9*), a result easily derived from the observation that this sequence forms a central hydrophobic core in the protein structure.

A peptide homolog of the HIV-1 Tat basic sequence region alone does not show full RNA binding activity. This activity is increased when the peptide is extended by amino acids from the core region (*10*). The ability of the peptides to discriminate between TAR mutants is dramatically reduced if the peptides contain fewer than five amino acids from the core region. From the EIAV Tat structure, it is clear that the hydrophobic core is a necessary structural domain presenting the RNA binding sequence to the TAR RNA at the protein surface. The five COOH-terminal residues of the core region are the necessary components for the formation of the turn around Gly[46]. Transcription factor TFIID binds to HIV-1 Tat, and the binding region extends from amino acids Val[36] to Gly[50] (EIAV Tat: Leu[39] to Ala[52]) with Lys[41] (EIAV Tat: Arg[43]) as a crucial component (*11*). The TFIID transcription factor thus binds to the only basic residue in the most stable domain of the protein.

The EIAV and HIV-1 Tat proteins seem to behave somewhat differently with respect to TAR binding (*12*). Figures 3 and 4 suggest that basic amino acids from the traditional RNA binding region (Arg[55] to Lys[63]), together with the NH_2-terminus (Arg[4] and Arg[5]) and the COOH-terminus (Arg[69]), form a positively charged cleft suitable for RNA binding. This cleft, stabilized by the hydrophobic core domain, was experimentally defined by NOEs from Asp[3], Pro[71], Tyr[73], and Leu[74] to the core domain. Indeed, a collapse of the tertiary structure upon the mutation of COOH-terminal residues, in particular Leu[74] and Leu[75], is suggested (*12*).

Although the EIAV Tat protein structure is flexible outside the core domain, it may adopt a more ordered structure on RNA binding (*13*). The disordered structure of the uncomplexed basic domain is readily understood in light of the high local charge density. Helical structure of the basic domain of HIV-1 Tat protein in the Tat-TAR complex has been suggested (*14*), but other experimental studies argue to the contrary (*15*). Verification or falsification of these hypotheses will have to wait until the structure of a Tat-TAR complex has been determined in atomic detail.

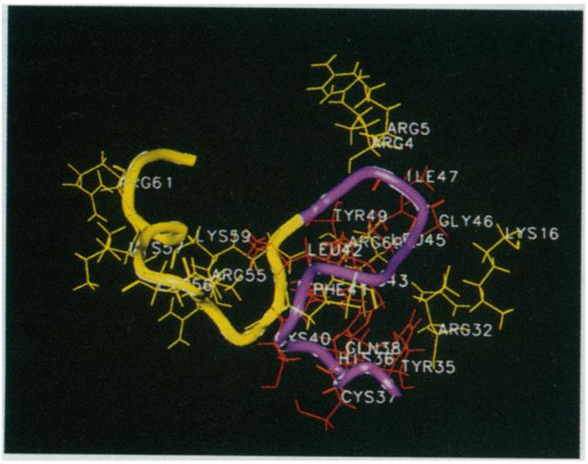

Fig. 3. Structure of the core domain and the basic domain of EIAV Tat protein. Shown are the side chains of the residues in the core domain that are conserved in Tat proteins according to Fig. 5 (red) and the basic amino acid side chains of the whole molecule (yellow). The specific structure displayed is one out of the six structures of Fig. 2. The basic domain is thus displayed as a static structure, which it is not according to the present results.

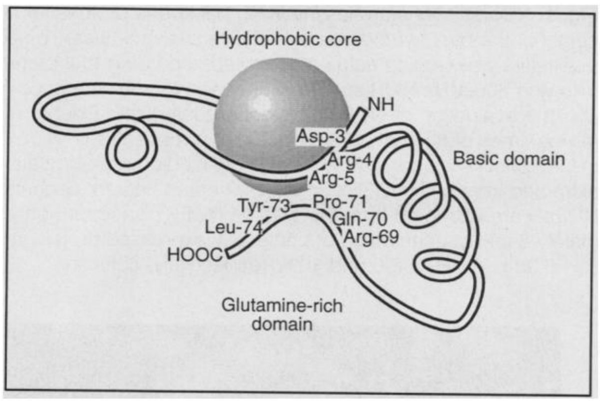

Fig. 4. Sketch of the general architecture of EIAV Tat protein. Indicated are the positions of the NH_2- and COOH-terminal residues showing NOEs to the core domain and the Arg residues at the NH_2- and the COOH-termini. These, together with the basic domain, build a positively charged cleft. Indicated are two regions with helix-forming tendency, according to Fig. 1, the third one being within the core domain. The figure is not meant to imply that these helices exist as stable structures in an appreciable fraction of the protein molecules.

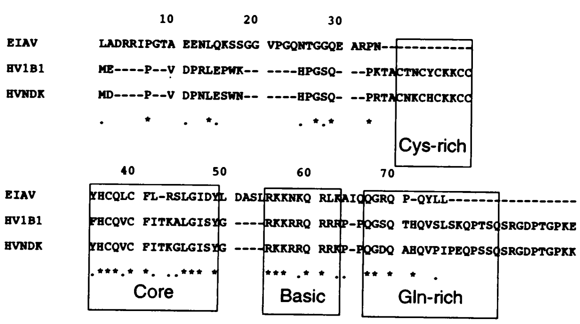

Fig. 5. Multiple sequence alignment of Tat proteins with the CLUSTAL V multiple-sequence alignment program with the use of the PAM100 matrix and standard parameters (*17*). The numbers on top correspond to the EIAV Tat numbering scheme. Along the side, HV1B1 is the HIV-1, B10, and HXB3 isolates and HVNDK is the HIV-1 and NDK isolates (*18*). Cys-rich, core, and basic regions are boxed according to (*2*). Amino acids are labeled with the one-letter convention (*16*). Asterisks mark identical amino acids; periods mark conservatively replaced amino acids.

REFERENCES AND NOTES

1. S. Noiman *et al.*, *Virology* **184**, 521 (1991).
2. P. Dorn *et al.*, *J. Virol.* **64**, 1616 (1990); D. Derse *et al.*, *ibid.* **65**, 7012 (1991); M. J. Gait and J. Karn, *Trends Biochem. Sci.* **18**, 255 (1994); J. D. Puglisi *et al.*, *Science* **257**, 76 (1992); M. G. Cordingley *et al.*, *Proc. Natl. Acad. Sci. U.S.A.* **87**, 8985 (1990).
3. L. W. Slice *et al.*, *Biochemistry* **31**, 12062 (1992).
4. K. M. Weeks *et al.*, *Science* **249**, 1281 (1990); D. W. Hoffman *et al.*, *Biochemistry* **32**, 1096 (1993).
5. D. Willbold *et al.*, *Biochemistry* **32**, 8439 (1993).
6. Both proteins were biologically active and showed the same level of activity in the chloramphenicol-acetyltransferase (CAT) assay. The samples with chemically synthesized EIAV Tat protein were prepared as described (*5*). Except for the early stages of the work, bacterially expressed protein was used for the NMR experiments. Samples of *Escherichia coli* BL21 (DE3) were transformed with the pET16b plasmid (Novagen, Madison, WI) containing the EIAV Tat sequence with an Ala[2] to Gly replacement and a 10-residue His leader sequence. The mutation did not influence activity. Cells from 6-liter fermenter runs were suspended in 5 mM imidazole, 500 mM NaCl, 20 mM tris-HCl (pH 7.9), and 6 M guanidinium chloride. The extract was passed over a 20-ml metal-chelating sepharose FF (Pharmacia, Freiburg, Germany) column with 50 mM $NiSO_4$ load buffer according to standard procedures. The resulting protein solution was concentrated to a total volume of approximately 5 ml. To obtain the Tat protein from the fusion protein, a standard

bromo-cyanide cleavage procedure was used because the leader sequence ended with a Met residue. The EIAV Tat protein was stored after lyophilization. Activity was tested after this procedure with a CAT assay (*5*).

7. Whereas the weak helix-forming tendency apparent in the NOESY cross-peak pattern does not materialize in all structure calculations, the protein forms stable helices simultaneously in the indicated regions (Fig. 1) in the presence of trifluoroethanol [H. Sticht *et al.*, *Eur. J. Biochem.* **218**, 973 (1993)].
8. A. T. Brünger, *X-PLOR, 3.1* (Yale Univ. Press, New Haven, CT, 1993).
9. A. P. Rice and F. Carlotti, *J. Virol.* **64**, 6018 (1990).
10. M. J. Churcher *et al.*, *J. Mol. Biol.* **230**, 90 (1993).
11. F. Kashanshi, *Nature* **367**, 295 (1993).
12. D. Derse and S. H. Newbold, *Virology* **194**, 530 (1992); R. Carroll, L. Martarano, D. Derse, *J. Virol.* **65**, 3460 (1991); R. Carroll, B. M. Peterlin, D. Derse, *ibid.* **66**, 2000 (1992).
13. Such behavior would be reminiscent of the bZIP DNA binding motifs [D. Patak and P. Sigler, *Curr. Opin. Struct. Biol.* **2**, 115 (1992); (*14*)]. If sequence regions with a helix-forming tendency (Fig. 1) formed helices simultaneously, the protein would be of the helix-loop-helix-turn-helix type, as is observed in trifluoroethanol solution (*7*). This motif is known from homeodomain proteins [A. Laughon, *Biochemistry* **30**, 11357 (1991)]. Homeodomain Arg-Lys^2 and Arg-Lys^3 residues, which contribute to DNA minor grove recognition, would then correspond to Arg^4 and Arg^5 of EIAV Tat protein in TAR minor grove recognition [K. M. Weeks and D. M. Crothers, *Cell* **66**, 577 (1991)].
14. B. J. Calnan *et al.*, *Genes Dev.* **5**, 201 (1991).
15. E. P. Loret *et al.*, *Biochemistry* **30**, 6013 (1991); E. P. Loret, P. Georgel, W. C. Johnson, P. S. Ho, *Proc. Natl. Acad. Sci. U.S.A.* **89**, 9734 (1992).
16. Single-letter abbreviations for the amino acid residues are as follows: A, Ala; C, Cys; D, Asp; E, Glu; F, Phe; G, Gly; H, His; I, Ile; K, Lys; L, Leu; M, Met; N, Asn; P, Pro; Q, Gln; R, Arg; S, Ser; T, Thr; V, Val; W, Trp; and Y, Tyr.
17. D. G. Higgins, A. J. Bleasby, R. Fuchs, *Comput. Appl. Biosci*, **8**, 189 (1992).
18. L. Ratner *et al.*, *Nature* **313**, 277 (1985); B. Spire *et al.*, *Gene* **81**, 275 (1989). Sequences are according to the Swiss-Prot protein data bank, release 27.
19. K. Wüthrich, *NMR of Proteins and Nucleic Acids* (Wiley Interscience, New York, 1986).
20. Distance information was extracted from NOESY spectra with mixing times of 150 and 300 ms. Sequential ($|i-j| = 1$) to medium-range ($1 < |i-j| \leq 5$) NOEs were extracted from the 150-ms spectra to avoid spin diffusion effects. Long-range NOEs ($|i-j| > 5$) were extracted from both NOESY spectra as well as from ^{15}N-^{1}H 3D heteronuclear multiple-quantum coherence (HMQC) spectra. Nuclear magnetic resonance data were evaluated with the NDee program package (*21*); 429 intraresidual ($|i-j| = 0$), 250 sequential ($|i-j| = 1$), 146 medium-range ($|i-j| = \leq 5$), and 34 long-range ($|i-j| > 5$) NOESY cross peaks could be assigned. A summary of the observed backbone cross peaks is given in Fig. 1. The structures were calculated from the NMR data according to the standard X-PLOR ab initio simulated annealing and refinement protocols with minor modifications. NOE cross peaks were grouped according to their intensity into three categories: strong (0.18 to 0.27 nm), medium (0.18 to 0.4 nm), and weak (0.18 to 0.55 nm). Starting from a template structure, 50 minimization steps were used, followed by 20-ps molecular dynamics at 1000 K with a soft-square NOE energy term (asymptote 0.1) and 10-ps molecular dynamics at 1000 K with increased weight on geometry and tilted asymptote (1.0) for the NOE energy term, cooling to 300 K in 50 K steps and 200 steps of minimization. Of the resulting 85 structures, the lowest energy structure was used as an input structure for a new round of ab initio calculation with identical protocol. The 11 structures from this second round of simulated annealing were subjected to molecular dynamics simulated annealing refinement, the energy function including an electrostatic term with a dielectric constant $\epsilon = 1$. Six structures were selected on the criteria of smallest number of NOE violations and lowest RMSD values and used for display in Fig. 2 and for calculation of the parameters in Table 1.
21. F. Herrmann *et al.*, unpublished results (the program is available on request).

22. We thank A. Gazit and A. Yaniv for their collaboration, and F. Herrmann for help with the ND program and artwork. Supported by the Fonds der Chemischen Industrie (FCI), an FCI grant (H.S. and D.W.), a MINERVA travel grant (D.W.), a grant from the Deutsche Forschungsgemeinschaft (P.R.), and the European Union BIOMED I–AIDS RESEARCH program.

7 February 1994; accepted 22 April 1994

Anergic T Cells as Suppressor Cells in Vitro

Giovanna Lombardi, Sid Sidhu, Richard Batchelor, Robert Lechler*

T cell–mediated suppression is an established phenomenon, but its underlying mechanisms are obscure. An in vitro system was used to test the possibility that anergic T cells can act as specific suppressor cells. Anergic human T cells caused inhibition of antigen-specific and allospecific T cell proliferation. In order for the inhibition to occur, the anergic T cells had to be specific for the same antigen-presenting cells (APCs) as the T cells that were suppressed. The mechanism of this suppression appears to be competition for the APC surface and for locally produced interleukin-2.

Evidence for T cell–mediated suppression has been derived from adoptive transfer systems in which T cells from an immunologically tolerant animal transfer tolerance to a naïve recipient animal if the T cells are injected together with specific antigen (*1*). Various models have been proposed to explain the mechanism of this T cell–mediated suppression. Suggestions that suppressor T cells represent a separate lineage and exert their effects through cascades of soluble factors have been discredited. Two current models exist. One model suggests that the effects are due to the suppressive effects of T cell–derived cytokines, such as interleukin-4 (IL-4), IL-10, or transforming growth factor–β (TGF-β), which inhibit the activation of IL-2–producing T cells (*2–4*). The other model proposes that antigen-specific T cells that have been rendered nonresponsive suppress other T cells that have the same specificity in a passive manner through competition for ligand and for cytokines such as IL-2 (*5*). We here provide in vitro evidence in support of the latter model.

Secretion of IL-2 by a subset of helper T lymphocytes (T_H1 cells) can be switched off as a result of partial signaling. This partial signaling can result from specific ligand recognition in the absence of costimulation (*6*), from receipt of full activation signals in the absence of IL-2–driven cell division (*7*), or from recognition of an altered ligand for which the T cell receptor has a lower affinity (*8*). T_H1 cells that have been turned off by these means are refractory to subsequent stimulation and are referred to as anergic. The induction of T cell anergy has been demonstrated in vitro (*6, 7, 9*) and in vivo (*10*). We test here whether or not anergic T cells have immunoregulatory effects on other T cells.

IL-2–secreting human T cell clones, specific for influenza hemagglutinin (HA) peptides [residues 100 through 115 (HC3) or 306 through 324 (HC6)] and restricted by HLA-DR1, were rendered anergic, by either incubation with soluble peptide in the absence of any added antigen-presenting cells (APCs) [as described (*9*)] or by incubation with immobilized antibody to CD3 (*11*). In response to the optimal stimulatory peptide concentration, these treatments led to >80% inhibition of T cell proliferation. The anergic T cells were added to cultures containing potentially reactive T cells, APCs, and antigen. Anergic T cells with the same specificity as the responsive T cells led to titratable inhibtion of proliferation (Fig. 1, A and B). This effect was specific because addition of an anergic clone with a different specificity (a third-party cell) caused less inhibition. No difference was seen in the degree of inhibition caused by T cells that had been rendered anergic by peptide or by antibody to CD3 (Fig. 1C).

Four possible mechanisms could contribute to this T cell–mediated suppression. First, it is possible that the anergic T cells, although unable to secrete IL-2, could be more lytic of the APC, thus depriving the responsive T cells of the opportunity to interact with ligand (*12*). Comparison of the lytic activity of the anergic and responsive T cells in a Cr release assay revealed that although the anergic T cells retained the ability to lyse antigen-bearing B cells, they were less efficient than the responsive T cells

Department of Immunology, Royal Postgraduate Medical School, London W12 ONN, UK.

*To whom correspondence should be addressed.